The local environment of Mn^{2+} impurities in $Rb_xCs_{1-x}CdF_3$ mixed crystals: a study with electron nuclear double resonance

1996 J. Phys.: Condens. Matter 8 7355

(http://iopscience.iop.org/0953-8984/8/39/012)

J. Phys.: Condens. Matter **8** (1996) 7355–7363. Printed in the UK

The local environment of Mn^{2+} impurities in $Rb_xCs_{1-x}CdF_3$ mixed crystals: a study with electron nuclear double resonance

F Lahoz†, R Alcalá†, Th Pawlik‡ and J-M Spaeth‡

† Instituto de Ciencia de Materiales de Aragón, Universidad de Zaragoza—CSIC, Zaragoza, Spain

‡ Fachbereich Physik, Universität-GH, Paderborn, Germany

Received 28 May 1996

Abstract. The electron paramagnetic resonance (EPR) and electron nuclear double resonance (ENDOR) of Mn^{2+} ions in $Rb_xCs_{1-x}CaF_3$ single crystals have been studied. A tetragonal phase similar to that in pure $RbCdF_3$ has been observed at 20 K in samples with $x = 0.95$, 0.9 and 0.8. The average rotational angle of the fluorine octahedra decreases when the Cs^+ content increases. ENDOR and double-ENDOR measurements on monodomain samples allow one to separate the contributions of Mn^{2+} centres with eight Rb^+ ions as next-nearest neighbours and with one Cs^+ and seven Rb^+ ions. An outwards relaxation of the axial fluorine close to the Cs^+ ion is detected.

1. Introduction

Electron paramagnetic resonance (EPR) studies of impurity centres in several mixed fluoroperovskite crystals have recently been reported [1–5]. These studies provide information on the local environments of the impurities as well as on the changes associated with structural phase transitions (SPT). Buzaré and Foucher [2] have investigated tetragonal Gd^{3+}–O^{2-} centres in $K_xRb_{1-x}CaF_3$ solid solutions with $x < 0.2$. In these crystals Gd^{3+} ions occupy a Ca^{2+} site and the O^{2-} ions occupy a nearest-neighbour (nn) F^- site. The next-nearest neighbours (nnn) are eight alkaline ions located at the corners of a cube. To explain the EPR spectra it has been proposed that there are different centres associated with the substitution for Rb^+ with K^+ in the nnn cube. The relative concentrations of these centres have been estimated by assuming a statistical distribution of the alkaline ions in the mixed crystals. The spin-Hamiltonian (SH) parameters of each of these centres are assumed to be independent of x. To account for the measured EPR spectra three types of centre were considered: those with the eight corners of the cube occupied by Rb^+ ions and those where one and two of the Rb^+ ions have been replaced by K^+.

Lahoz *et al* [5] have studied Mn^{2+} centres in $Rb_xCs_{1-x}CaF_3$ and $RbCa_xCd_{1-x}F_3$ for $0 < x < 1$. Mn^{2+} enters in a substitutional Ca^{2+} site. In this case the experimental results, even in the case of crystals with x-values either close to 0 or close to 1, could not be explained with a superposition of spectra due to a few types of Mn^{2+} centre. A distribution of centres with slightly different SH parameters was necessary. No precise information about this distribution could be obtained from EPR data.

In an effort to understand the local disorder around Mn^{2+} ions in mixed fluoroperovskites and to investigate the presence of different types of Mn^{2+} centre, the EPR studies reported

0953-8984/96/397355+09$19.50

in reference [5] have been extended to $Rb_xCs_{1-x}CdF_3$ mixed crystals ($0.6 < x < 1$) and complemented with ENDOR measurements. It has been previously found in some ENDOR studies of Mn-doped $RbCdF_3$ and $RbCaF_3$ [6–8] that this technique allows one to determine small changes in the Mn^{2+} environment (associated with a SPT) that were barely discernible in the EPR spectra. Both EPR and ENDOR results are reported and discussed in the present paper.

2. Experimental details

Single crystals of $Rb_xCs_{1-x}CdF_3$:Mn were grown by the Bridgman method in a radio-frequency- (rf-) heated furnace using vitreous carbon crucibles. Mn^{2+} was incorporated as MnF_2. The MnF_2 content in the starting materials ranged from 0.01 to 0.05 mol%.

The nominal composition of the mixed crystals was $x = 0.95$, 0.9, 0.8 and 0.7. All of them were analysed by atomic emission spectroscopy. The results are $x = 0.95$, 0.9, 0.8 and 0.6. Monodomain samples were prepared by producing crystals with a cylindrical shape with the axis along one of the ⟨100⟩ directions and inserting them into cylindrical Teflon tubes. The tube presses the sample and when the structural phase transition (SPT) takes place, domains are preferentially induced with the tetragonal axis along the axis of the cylinder.

EPR and stationary ENDOR measurements were performed with a computer-controlled X-band spectrometer (9.5 GHz) at temperatures between 20 K and 300 K. Double-ENDOR measurements [9] were performed in the same ENDOR set-up using two radio-frequencies f_1 and f_2. f_1 was set to a particular ENDOR line and its amplitude was modulated at 800 Hz while f_2 was swept through the range of interest and its amplitude was modulated at 5 Hz. Two lock-in amplifiers (800 Hz and 5 Hz) in series detected the double-ENDOR signal.

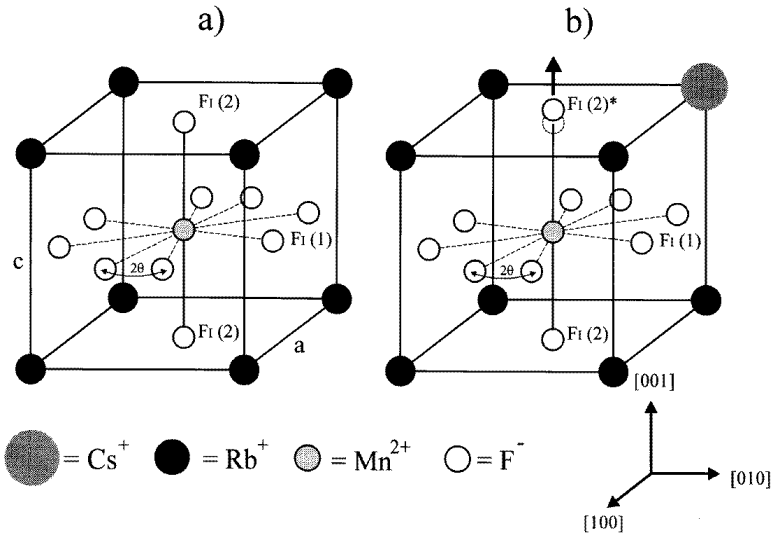

Figure 1. (a) The Mn^{2+} environment in the tetragonal phase of $RbCdF_3$. The two possible rotations of the fluorine octahedra around the [001] axis are shown. *a* and *c* are the pseudo-cubic lattice parameters. (b) The proposed arrangement of the FI(2) nuclei in the C_1 centre.

3. Experimental results

The EPR of Mn^{2+} in $RbCdF_3$ was reported previously [10]. From the analysis of the angular evolution of the Mn^{2+} lines it was concluded that Mn^{2+} ions enter in a Cd^{2+} site. The line positions at room temperature (RT) were explained with the usual spin Hamiltonian (SH):

$$H = g\mu_B \boldsymbol{B}\cdot\boldsymbol{S} + \boldsymbol{S}\mathbf{A}\boldsymbol{I} + \frac{a}{120}\{O_4^0 + 5O_4^4\} + \sum_i \boldsymbol{S}\mathbf{A}_i\boldsymbol{I}_i \qquad (1)$$

with $S = 5/2, I = 5/2$ and $I_i = 1/2$. The first term represents the electronic Zeeman energy, the second one expresses the hyperfine interaction (HF) with the ^{55}Mn ($I = 5/2$) nucleus, the third one gives the fourth-order crystal-field contributions and the fourth term corresponds to the superhyperfine interaction (SHF) with the nearest-neighbour ^{19}F ($I = 1/2$) nuclei. At 124 K $RbCdF_3$ undergoes a cubic-to-tetragonal SPT that consists of an alternated rotation of the fluorine octahedra around one of the $\langle 100\rangle$ directions together with an elongation along the rotation axis. The corresponding local structure around Mn^{2+} ions is shown in figure 1(a). The SPT produces detectable shifts in the positions of the lines corresponding to the transitions from $m_s = \pm 5/2$ to $m_s = \pm 3/2$ and from $m_s = \pm 3/2$ to $m_s = \pm 1/2$ but not in the lines associated with the transition from $m_s = 1/2$ to $m_s = -1/2$. These changes can be accounted for by adding a second-order crystal-field term $(D/3)O_2^0$ to the SH given in equation (1). D-values obtained from the fitting of the calculated line positions to the experimental ones at different temperatures have been used to monitor the SPT [7, 10].

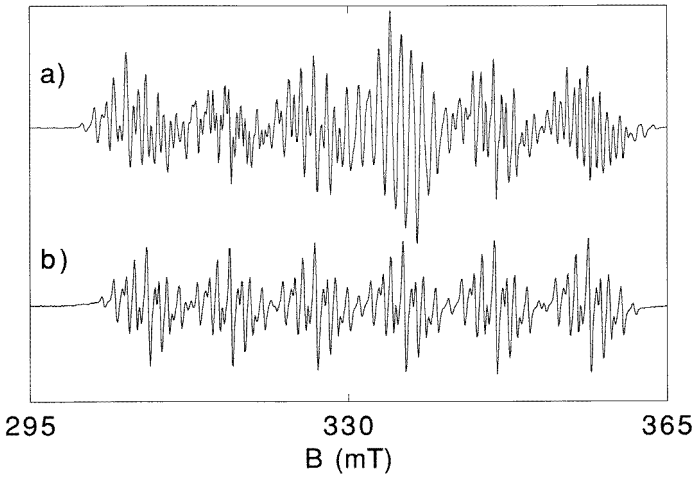

Figure 2. The EPR of Mn^{2+} in (a) $RbCdF_3$ and (b) $Rb_{0.9}Cs_{0.1}CdF_3$ crystals, measured at 20 K with the external magnetic field $\boldsymbol{B}$ along a $\langle 100\rangle$ direction. The DPPH g-value (2.0037) corresponds to 329.3 mT.

The EPR spectrum of Mn^{2+} in $Rb_xCs_{1-x}CdF_3$ crystals ($1 \geqslant x \geqslant 0.6$) has been measured at different temperatures and for different orientations of the applied magnetic field $\boldsymbol{B}$. The spectrum is almost the same for all of the solid solutions but different from the one for pure $RbCdF_3$. The behaviour is very similar to that found for $Rb_xCs_{1-x}CaF_3$ [5]. We show in figure 2 the Mn^{2+} EPR spectra of $RbCdF_3$ and of $Rb_{0.9}Cs_{0.1}CdF_3$ crystals measured at RT with the static magnetic field along one of the $\langle 100\rangle$ directions. There are six groups

of lines due to the HF interaction with the Mn nucleus. The structure in each of the six HF groups is caused by the SHF interaction with the nearest-neighbour fluorine nuclei. In pure $RbCdF_3$ at RT the transitions from $m_s = \pm 5/2$ to $m_s = \pm 3/2$ and from $m_s = \pm 3/2$ to $m_s = \pm 1/2$ are shifted from the transition from $m_s = +1/2$ to $m_s = -1/2$ due to the effects of the cubic crystal field. They are superimposed partly on the latter transitions and therefore not clearly seen as HF–SHF sextets (figure 2(a)).

In the mixed crystals, even for values of x as high as 0.95 or 0.9, only the transitions from $m_s = +1/2$ to $m_s = -1/2$ are seen (figure 2(b)). In order to explain this, we propose that there are strains in the mixed crystal which produce a distribution of low-symmetry crystal fields around each Mn^{2+} resulting in a broadening of the line groups corresponding to the transitions from $m_s = \pm 5/2$ to $m_s = \pm 3/2$ and from $m_s = \pm 3/2$ to $m_s = \pm 1/2$ because of second-order zero-field-splitting terms. The lines corresponding to the transition from $m_s = +1/2$ to $m_s = -1/2$ are unaffected by the broadening effects and can, therefore, be seen. Our ENDOR results qualitatively confirm this explanation (see below).

ENDOR measurements have been taken at 20 K on $Rb_xCs_{1-x}CdF_3$:Mn samples with $x = 0.95$, 0.9, 0.8 and 0.6. For the ENDOR measurements the magnetic field was set into the line group belonging to $m_I(^{55}\mathrm{Mn}) = -1/2$.

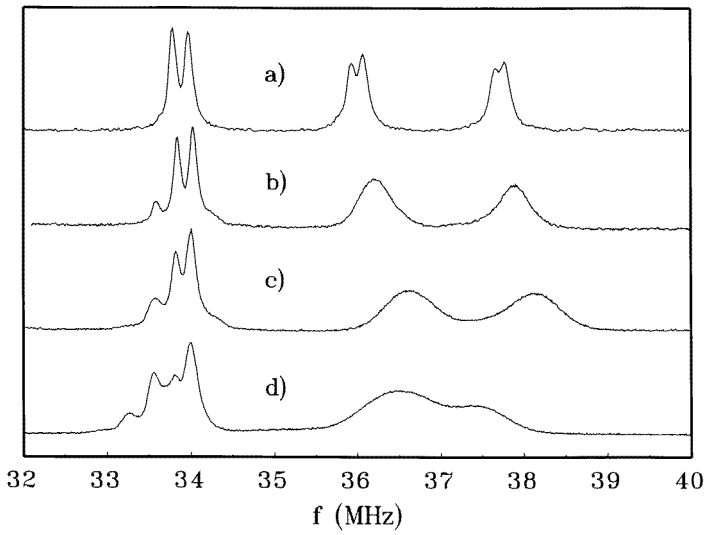

Figure 3. ENDOR spectra of Mn^{2+} in $Rb_xCs_{1-x}CdF_3$ monodomain samples with the domain axis along the [001] direction: (a) $x = 1$; (b) $x = 0.95$; (c) $x = 0.9$; (d) $x = 0.8$; measured at 20 K with $\boldsymbol{B}$ in the plane (001) at 28° from the [100] direction.

Figure 3 shows ENDOR spectra with $\boldsymbol{B}$ in the (001) plane, being approximately 28° away from the [100] direction of monodomain samples, with the axis along the [001] direction taken at 20 K. In figure 3, trace (a), the measured spectrum of pure $RbCdF_3$ is shown, while traces (b) to (d) represent spectra for mixed crystals with $x = 0.95$, 0.9 and 0.8. First, the lines for pure $RbCdF_3$ will be discussed. All of the lines are due to F nearest neighbours. Around 34 MHz they are due to the FI(2) nuclei, while those between 36 and 38 MHz are due to FI(1) nuclei (see figure 1(a)). To first order the ENDOR frequencies are given by

$$h\nu = |m_s A(\Theta) - g_I \mu_n B_0| \tag{2}$$

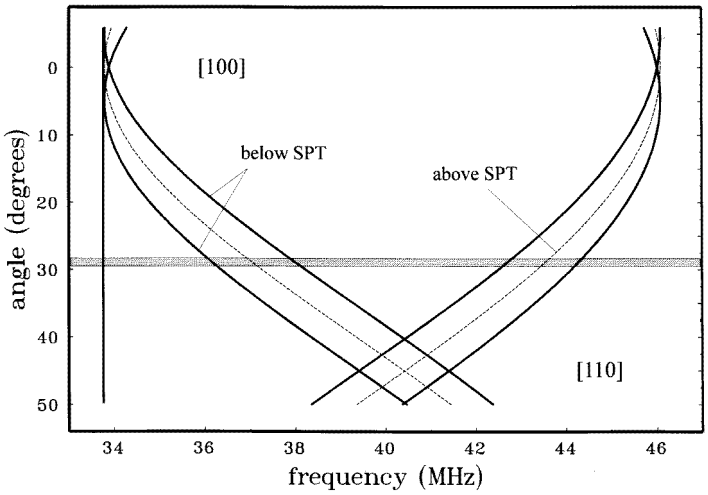

Figure 4. Calculated angular dependences of the FI(1) and FI(2) nearest-neighbour ENDOR lines of a monodomain sample with the domain axis along the [001] direction. The magnetic field is rotated in the (001) plane. The horizontal bar marks the orientation for the ENDOR measurements of figure 3.

where $A(\Theta)$ is the angle-dependent SHF interaction constant and the second term is the Larmor frequency of the ^{19}F nuclei [9]. The F SHF tensors are axially symmetric; their axes point to the Mn^{2+} nucleus [7]. The angular dependence of the ENDOR lines for rotation of the magnetic field in the (001) plane is shown in figure 4. The orientation used in figure 3 is indicated by a horizontal bar (28° off the ⟨100⟩ direction). There would be two lines (for $m_s = -1/2$) due to the FI(1) nuclei above the SPT at 124 K (the broken lines in figure 4), which split due to the rotation of the F octahedra below the SPT. The splitting is given by the rotation angle [7]. In figure 3, only the two FI(1) lines at lower frequencies are shown. The line at around 34 MHz is due to the two FI(2) nuclei (figure 1(a)). All of the lines in figure 3(a) are due to pairs of equivalent F nuclei and display a small splitting (not shown in figure 4), which was explained in $RbCaF_3$ as being a consequence of second-order SHF interactions [8].

Comparison of the ENDOR spectra of the mixed crystal reveals two features.

(i) The FI(2) spectrum contains new lines and the FI(1) lines become broader and their splitting due to the rotation becomes increasingly smaller with increasing values of x, i.e. when the substitution of Cs^+ for Rb^+ becomes more frequent.

(ii) The ENDOR lines at 46 MHz (see figure 4) for FI(1) nuclei for $\boldsymbol{B}\|[100]$ are not broadened in the mixed crystals and are about as narrow as those of the FI(2) nuclei. This indicates that the broadening in the other orientations is due to a superposition of different Mn^{2+} centres with a variation of the rotational angle as a consequence of the Cs^+ mixing and possibly due to some other influence on the angle due to the Cs^+ doping.

In the angular dependence of the lines of the FI(1) nuclei, there are no further line splittings. One can only determine the SHF interactions from the peaks of the broadened lines. It turns out that they are within experimental error the same as those for the unperturbed centres: for $x = 0.95$ and 0.9 the isotropic SHF constant $a/h = 47.8$ MHz and the anisotropic SHF constant $b/h = 8.5$ MHz. The rotation angle measured at 20 K

differs, though. Its average value decreases from 4.72° at $x = 1$ to 4.5 at $x = 0.95$ and 3.9° at $x = 0.9$.

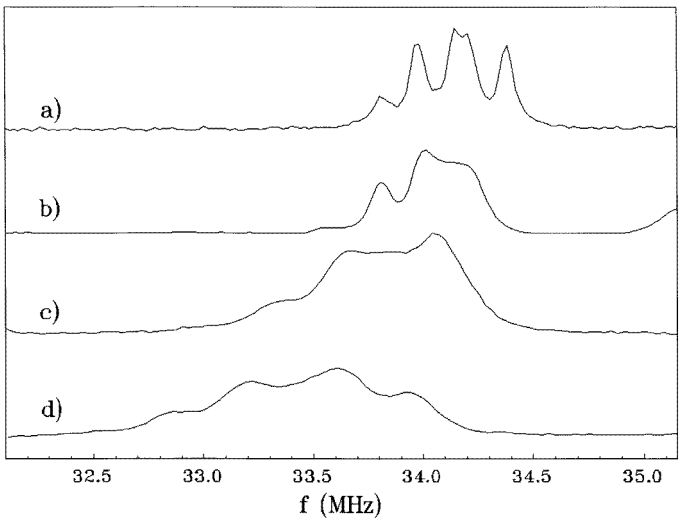

Figure 5. The 34 MHz region of the ENDOR spectrum of Mn^{2+} in a multidomain sample of $Rb_xCs_{1-x}CdF_3$: (a) $x = 1$; (b) $x = 0.95$; (c) $x = 0.8$; (d) $x = 0.6$; measured at 20 K with $\boldsymbol{B}$ in the plane (001) at 20° from the [100] direction.

Figure 5 shows the ENDOR lines of FI(2) nuclei at around 34 MHz in a multidomain sample ($\boldsymbol{B}$ is about 20° off the [100] direction in the (001) plane). Trace (a) is from a pure $RbCdF_3$ crystal, while traces (b) to (d) are for $x = 0.95$, 0.8 and 0.6 crystals. The one for $x = 0.9$ is not shown because it is almost the same as that of $x = 0.95$. In pure $RbCdF_3$ the group of lines are a superposition of three doublets, each of which is due to a pair of equivalent FI(2) nuclei, with a second-order SHF splitting of about 0.2 MHz. The three groups correspond to the three domains. In the mixed crystals, a broadening of the lines is also observed when x decreases, but some structure remains. Together with the broadening, a shift of the lines towards lower frequencies is observed, indicating a decrease of the SHF interaction. Such a decrease could occur as a consequence of an increase of the Mn^{2+}–F distance in the mixed configuration (see section 4).

The three ENDOR lines measured for $x = 0.95$ at 34 GHz in the monodomain sample (figure 3, trace (b)) indicate that a superposition of probably two different centres, one unperturbed and one with one Cs^+ ion in the next-nearest shell, are superimposed. In order to identify the lines of the two centres, we performed double-ENDOR experiments. Figure 6, trace (a), shows the ENDOR transitions of FI(2) nuclei at 34 MHz for $m_s = -1/2$ and at 44 MHz for $m_s = 3/2$ (see equation (2)). In the double-ENDOR experiment, one radio-frequency f_1 is tuned to one line in the 34 MHz group (marked by an asterisk in figure 6, traces (b) to (d)), while the other one is swept through the 44 MHz region. It is a virtue of double ENDOR that all lines appearing in the double-ENDOR spectrum must be due to nuclei coupled to the same unpaired electron, i.e. must belong to the same centre. When f_1 is set at the ENDOR line at the highest frequency of the group at 34 MHz (figure 6, trace (b)), all three lines appear in both the 44 MHz and 34 MHz group. When f_1 is tuned to the following line towards lower frequency (figure 6, trace (c)), only the two ENDOR lines at

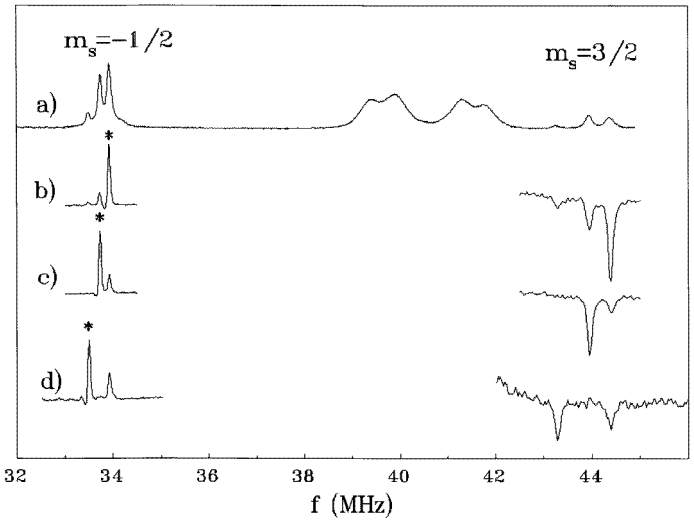

Figure 6. Double-ENDOR measurements of Mn^{2+} in a monodomain sample of $Rb_{0.95}Cs_{0.05}CdF_3$ with the domain axis along the [001] direction: (a) ENDOR spectra in the 34 MHz and 44 MHz regions; (b), (c) and (d): double-ENDOR spectra obtained with the frequency f_1 tuned to the line marked with an asterisk in each of the spectra; measured at 20 K with $\boldsymbol{B}$ in the plane (001) at 40° from the [100] direction.

higher frequencies appear in each group. When f_1 is set to the lowest-frequency ENDOR line, f_2 shows the two lines at lowest and highest frequencies in the 44 MHz and 34 MHz region (figure 6, trace (d)).

From these results we can conclude that there are two centres that contribute to the ENDOR signal in both the 34 MHz and the 44 MHz region. One of these centres gives lines at 33.8 and 34 ($m_s = -1/2$) and 43.8 and 44.4 MHz ($m_s = 3/2$) while the lines due to the other one appear at 33.5 and 34 ($m_s = -1/2$) and 43.2 and 44.4 MHz ($m_s = 3/2$). The intensity of the signal due to the first of these centres is higher than that of the second one. Besides this, the positions of the lines corresponding to the first centre coincide with those in pure $RbCdF_3$. Thus, the first centre is the unperturbed Mn^{2+} centre; the other one must be a perturbed one.

4. Discussion

From both ENDOR and double-ENDOR measurements it is clear that in the mixed crystals a superposition of different defects is seen in the spectra. When assuming a statistical distribution of Rb^+ and Cs^+ in the next-nearest-neighbour shell, one would expect for the $x = 0.95$ sample 66% of unperturbed centres (C_0) and 28% of centres with one Cs^+ in the second shell (C_1 centres). The double-ENDOR lines which coincide with those of $RbCdF_3$ are those of C_0 defects. The splitting of these lines is 0.2 MHz, which is explained by the second-order SHF interactions [8]. The other line pair at 34 MHz is due to C_1 defects and has a bigger splitting of 0.5 MHz. The reason for this is that the two FI(2) nuclei are not equivalent any more. Since the lowest-frequency line at around 34 MHz is part of the C_1 spectrum, the SHF interaction of one of the FI(2) fluorines must have become smaller. We propose that the FI(2) close to the Cs^+ ion in the C_1 centres undergoes a small outwards

relaxation while for the other FI(2) ion the Mn^{2+}–F^- distance remains almost the same as in the C_0 centres (figure 1, trace (b)). The doublet splitting is due to both the different SHF interactions of the two FI(2) nuclei and some second-order effects. The structural model for the C_1 centre as regards the two axial FI(2) nuclei is shown in figure 1(b). We cannot say from the experiment whether the isotropic SHF constant, the anisotropic SHF constant or both have decreased for one of the two FI(2) nuclei in the perturbed centre. We think that it is the isotropic constant for the following reason: in pure $CsCdF_3$ a/h is about 4 MHz smaller than in $RbCdF_3$ [11], while the values of b/h are practically identical for $CsCdF_3$ and $RbCdF_3$.

Similar conclusions can be drawn for the $Rb_{0.9}Cs_{0.1}CdF_3$ crystals, for which the only difference in the ENDOR spectrum is a slight increase of the relative intensity of the signal due to C_1 centres (see figure 3) as a consequence of the larger Cs^+ concentration. In these crystals, C_2 centres will be present with a probability of about 0.15, but we do not see any new line that can be associated with them. This can be understood because in these C_2 centres the probability for the fluorines in the [001] direction of having only one Cs^+ as nn is about 0.07 and, in this case, its SHF interaction can be similar to that of the outwards-relaxed fluorine in the C_1 centres. Thus, the probability of having an [001] F^- ion with two nn Cs^+, that could give new ENDOR lines, is only about 0.08. Besides, it would be possible to have the two Cs^+ in adjacent or opposite corners of the face of the cube that contains the FI(2) ion and this could produce slightly different relaxations in the fluorine introducing an extra broadening of the line. In the $x = 0.8$ sample the probability for C_2 centres having an [001] F^- ion with two nn Cs^+ is 0.17. The low-frequency line at 33.25 MHz that appears in figure 3, trace (d), could therefore be due to FI(2) nuclei of C_2 centres with two Cs^+ in the nn position.

With the results from ENDOR and double-ENDOR measurements on the monodomain samples one can now explain the intermediate spectrum of the multidomain sample at $x = 0.6$ (figure 5, trace (d)) qualitatively in the following way.

It is seen from figure 5 that for $x = 0.6$ the FI(2) ENDOR lines shift to lower frequencies and thus to lower SHF interactions. For the pure $CsCdF_3$ the lines belonging to the FI(2) nuclei would be expected at 32.1 MHz. For the pure $RbCdF_3$ in figure 5 they appear at around 34.1 MHz.

At $x = 0.6$ essentially one has C_2 , C_3 and C_4 centres (two, three and four Cs^+ ions in the second shell). The probability for C_0 and C_1 centres is very low. The FI(2) nuclei of C_2, C_3 and C_4 centres should have even smaller SHF constants and the ENDOR lines should therefore appear at lower frequencies. In addition to these different local structures around Mn^{2+} there is also an influence of distant Cs^+ ions: the higher concentration of Cs^+ leads to an increase of the lattice constant ($a = 4.395$ Å in $RbCdF_3$ compared to $a = 4.47$ Å in $CsCdF_3$) and this also influences the FI(2) SHF interactions.

From the fact that for $\boldsymbol{B}\|[100]$ the line width of the FI(1) ENDOR lines is almost the same as that for FI(2) nuclei also in the mixed crystals, we assume that the line broadening at other orientations is due to a superposition of centres with different rotation angles. At $x = 0.95$, for example, the ENDOR spectrum could be due to the superposition of lines corresponding to C_1 and C_0 defects with different rotation angles, but we cannot decide whether the rotation angles are also influenced by strains caused by Cs^+ in the neighbourhood further away from the Mn^{2+} defect. For smaller x-values it is seen that the average rotation angle decreases and the width of the distribution of angles increases.

It is noted that the inclusion of Mn^{2+} diminishes the rotation angle from 7° in pure $RbCdF_3$ to 4.72° at 20 K. The incorporation of Cs^+ apparently influences this value in addition. The lack of further structure of the ENDOR lines prevented, however, a more

detailed analysis.

The fact that we measured ENDOR lines for $m_s = 3/2$ shows that the assumption made when discussing the EPR spectrum of the mixed crystals, that the higher-m_s transitions are broadened and not seen, is correct. These transitions were also saturated and showed an ENDOR effect.

Acknowledgments

This work was supported by the CICYT (Spain) under Project No MAT-92-1279. The financial support of the Stiftung Volkswagenwerk and the Spanish–German Cooperation Committee is also acknowledged.

References

[1] Foucher P, Buzaré J Y, Ridou C, Rousseau M and Hennion B 1990 *Ferroelectrics* **107** 325
[2] Buzaré J Y and Foucher P 1991 *J. Phys.: Condens. Matter* **3** 2535
[3] Minorel A M, Silly G and Buzaré J Y 1991 *Ferroelectrics* **124** 297
[4] Debaud-Minorel A M and Buzaré J Y 1994 *J. Phys.: Condens. Matter* **6** 2189
[5] Lahoz F, Alonso P J, Villacampa B and Alcalá R 1995 *Radiat. Effects Defects* **135** 163
[6] Studzinski P and Spaeth J-M 1983 *Radiat. Effects* **73** 207
[7] Studzinski P and Spaeth J-M 1986 *J. Phys. C: Solid State Phys* **19** 6441
[8] Lahoz F, Alonso P J, Alcalá R, Pawlik T and Spaeth J-M 1995 *J. Phys.: Condens. Matter* **7** 8637
[9] Spaeth J-M, Niklas J K and Bartram R H 1992 *Structural Analysis of Point Defects in Solids (Springer Series in Solid-State Sciences 43)* (Berlin: Springer)
[10] Studzinski P 1986 *PhD Thesis* University of Paderborn
[11] Ziaei M E 1977 *PhD Thesis* Oxford University